Journal of Food Engineering 192 (2017) 79–92

Contents lists available at ScienceDirect

Journal of Food Engineering

journal homepage: www.elsevier.com/locate/jfoodeng

Finite element modeling of continuous-flow microwave heating of fluid foods and experimental validation

Sezin Tuta [a, *], T. Koray Palazoğlu [b]

[a] Çankırı Karatekin University, Faculty of Engineering, Department of Food Engineering, 18100, Çankırı, Turkiye
[b] University of Mersin, Faculty of Engineering, Department of Food Engineering, 33343, Mersin, Turkiye

ARTICLE INFO

Article history:
Received 4 March 2016
Received in revised form
15 June 2016
Accepted 10 August 2016
Available online 11 August 2016

Keywords:
Fluid food products
Microwave heating
Helical tube configuration
Numerical modeling
Temperature distribution

ABSTRACT

In this study, heating of fluid foods in a specially designed continuous-flow microwave heating unit (915 MHz and 5 kW maximum power) was simulated by finite element method using COMSOL Multiphysics. Experiments were then conducted with different test fluids (distilled water, 0.5% and 1% CMC solutions) at different flow rates (1, 2, 3 L/min) to validate the model. The pilot-scale unit consisted of a PTFE tubing which was helically configured within cylindrical cavity of the unit. Cross-sectional temperature distribution at the exit of the tube was measured by specially designed thermocouple system at thirteen points. Numerical and experimental results showed that heating was more uniform for distilled water in comparison to CMC solutions at all flow rates. A comparison of the results of this study to the literature showed that more uniform heating can be achieved for high-viscosity fluid food products by using helical tube in continuous-flow microwave heating systems.

1. Introduction

Pasteurization/sterilization of fluid food products can be carried out either by aseptic processing or canning. Although canning is the dominant technology used by the food industry, it is known to result in extensive damage to quality and nutrients in case of highly viscous products due to the slow rate of heat transfer. Aseptic processing (continuous-flow heating) has the potential to improve product quality and reduce nutrient losses by allowing for heating rapidly and uniformly in comparison to canning. However, despite these advantages, non-uniform heating of highly viscous fluid foods in conventional aseptic processing systems (heat exchangers) still remains a problem. Volumetric heating may eliminate this drawback of conventional heat exchangers. Microwave energy provides volumetric heating by generating heat throughout the volume as a result of molecular interaction with the electromagnetic field (Thostenson and Chou, 1999). Continuous-flow microwave heating is a novel and emerging technology that can be used for heating fluid food products volumetrically. Fresh-like quality products can be made by using continuous-flow microwave heating systems through rapid and volumetric heating. In addition to these, absence of hot surfaces in microwave heating units also presents an advantage especially for heat sensitive products.

Earlier research showed that uniform temperature distribution can be achieved by continuous-flow microwave heating of low-viscosity fluid products such as apple juice (Gentry and Roberts, 2005; Tajchakavit et al., 1998), orange juice (Nikdel et al., 1993; Tajchakavit and Ramaswamy, 1995) and milk (Coronel et al., 2003; Sierra et al., 1999; Valero et al., 2000; Villamiel et al., 1996). Existing continuous-flow microwave systems show that narrow temperature distribution can readily be achieved for low-viscosity foods but non-uniform heating still remains a problem for highly viscous foods. Non-uniform temperature distribution in a continuous-flow microwave system was reported for sweet potato puree (Coronel et al., 2005; Steed et al., 2008), green pea/carrot puree (Kumar et al., 2008) and 0.5% CMC solution (Salvi et al., 2009). Uneven temperature distribution in highly viscous fluid foods occurs due to non-uniform distribution of electric field inside the cavity. Diameter and configuration of the applicator tube and dielectric properties of the fluid are also important parameters. Microwave power, flow rate and temperature also affect temperature distribution in the product (Kumar et al., 2008; Romano and Apicella, 2015). For viscous fluids, conduction is the major mode of heat transfer and no mixing takes place within fluid which in turn results in regions that are over-heated. Generally, to overcome non-uniform temperature distribution problem, approaches such

* Corresponding author.
E-mail address: sezintuta@hotmail.com (S. Tuta).

http://dx.doi.org/10.1016/j.jfoodeng.2016.08.003
0260-8774/

as generating turbulent flow, installing static mixers or using curved tubes instead of straight tubes may be used (Koutsky and Adler, 1964). Coronel et al. (2005) and Kumar et al. (2008) employed static mixers in order to solve this problem during continuous-flow microwave heating, and they reported that mixing effect caused by static mixers improved temperature uniformity. Difficult and time consuming cleaning due to complex geometry of static mixers causes contamination risk and limits usage of these devices in food processing systems (Eesa, 2009).

Using helical tubes instead of straight tubes is another technique for improving heating uniformity in continuous systems. Helical tubes have been widely used in industrial applications such as heat exchangers, chemical reactors, and piping systems. Heating and cooling of high-viscosity or shear-sensitive products can be achieved by using helical tubes (Kumar et al., 2006). Helical tubes are known to enhance heat transfer by introducing secondary flow. Degree of secondary flow is characterized by Dean number ($Dn = Re\sqrt{d/D}$), where d is the inside diameter of the tube and D is the diameter of the helical coil). Secondary flow is reported to promote the uniformity of heating by causing radial mixing (Castelain and Legentilhomme, 2006; Koutsky and Adler, 1964; Palazoğlu and Sandeep, 2004). Few studies reported on using helical tubes in microwave systems (Gentry and Roberts, 2005; Nikdel and MacKellar, 1992; Nikdel et al., 1993; Tajchakavit and Ramaswamy, 1995). In these studies, low-viscosity fluids were heated in lab-scale units and after heating treatment microbial and enzyme properties of products were investigated.

No study up to date has explored the effect of using a helical tube on temperature distribution in a continuous-flow microwave system. In the present study, a pilot-scale continuous-flow microwave heater (915 MHz, maximum power of 5 kW) was built to this purpose and the effect of helical configuration on heating characteristics of different test fluids was studied both experimentally and numerically. Experiments and simulations were conducted with distilled water, 0.5% and 1% CMC solutions at a power of 4 kW and at flow rates of 1, 2, 3 L/min. Finite element model of the system was developed in COMSOL Multiphysics and model validation was carried out by comparing experimental temperature measurements to the computed temperatures.

2. Material & methods

2.1. Material

Distilled water and carboxymethyl cellulose (CMC) solutions (0.5 and 1.0% w/w) were used as Newtonian and non-Newtonian test fluids. Carboxymethyl cellulose solutions were prepared by dissolving CMC powder (Prosis, Istanbul, Turkiye) in distilled water at room temperature. The solutions were stored at 4 °C for two days to totally dissolve the clumps and to allow for removal of the air bubbles. The test fluids were brought to 20 ± 1 °C before each run.

2.2. Methods

2.2.1. Dielectric and physical properties of test fluids

Dielectric properties of distilled water and CMC solutions were calculated using the equations given by Komarow and Tang (2004) and Coronel et al. (2008), respectively. Thermophysical properties (thermal conductivity, specific heat and density) were calculated from Choi and Okos correlations (Toledo, 1994). Loss tangent value (tan δ) and penetration depth (D_p) were calculated from Eqs. (1) and (2), respectively.

$$\tan\delta = \varepsilon'' \Big/ \varepsilon' \tag{1}$$

$$D_p = \frac{\lambda}{2\pi\sqrt{2\varepsilon'\left[\sqrt{1+\left(\frac{\varepsilon''}{\varepsilon'}\right)^2}\right]-1}} \tag{2}$$

where λ is wavelength in free space (m), ε' is dielectric constant and ε'' is dielectric loss factor. Dynamic viscosity of distilled water was obtained from literature (Geankoplis, 1993). Determination of rheological properties of CMC solutions were carried out experimentally by using a rotational viscometer (Brookfield DV-II+ProEXTRA, USA). Carboxymethyl cellulose was modeled as a pseudoplastic fluid (n < 1) whose flow behavior can characterized by the Power-Law model (Eq. (3)).

$$\sigma = K\,\dot{\gamma}^n \tag{3}$$

where σ is shear stress (Pa), $\dot{\gamma}$ is shear rate (1/s). K and n represent material constants, namely the consistency coefficient and flow behavior index, respectively. K and n values were determined between 20 and 90 °C and experiments were carried out in triplicate.

2.2.2. Continuous-flow microwave system

Continuous flow microwave system (Sonar, Izmir, Turkiye) consisted of a 5 kW magnetron operating at 915 MHz, a rectangular waveguide and a cylindrical cavity (Fig. 1-a1). Polytetrafluoroethylene (PTFE) tubing of the system was helically coiled within the cavity. Generally, such tubings are internally corrugated for easy shaping but this disturbs flow pattern of the fluid. Smooth interior tubing (Bioflex PTFE Liner, Aflex Hose Ltd., West Yorkshire, England) was chosen to eliminate this drawback and to maintain laminar flow profile. The tubing had rib sections on the outside that support the tube against kinking. Inside and outside diameters of tubing were 0.038 m and 0.040 m, respectively. Vertical rise of the tubing was 0.124 m per unit length. Curvature ratio of the helical coil (d/D; ratio of inside diameter of tube to diameter of coil, where the diameter of the coil is measured from tube-centerline to tube-centerline) was 0.105. The length of tubing inside the cavity (microwave exposure region) was 1.54 m. Test fluids were pumped through the system by a progressive cavity pump (Inoxpa, Spain) with an adjustable speed motor.

2.2.3. Experimental methods

2.2.3.1. Temperature measurement. Temperature distribution at the exit of the cavity were obtained by using a specially designed thermocouple assembly in which thirteen 36 gauge type-T thermocouples (Omega Engineering, Inc., Stamford, CT) were cross-sectionally distributed as shown in Fig. 1-a2. To measure the inlet temperature, a thermocouple was placed through the gasket at the entrance of tube. Temperatures were monitored with 1 s interval by using a data acquisition system (Model DT9805, Superlogics, Inc., Waltham, MA).

Temperature readings at all thirteen locations were recorded when steady state was reached which was indicated by constant temperatures at all locations. The system was run at a power of 4 kW, and the flow rates of test fluids were 1, 2, and 3 L/min (0.0147 m/s, 0.0294 m/s and 0.0441 m/s). The average residence times of the test fluids for flow rates of 1, 2, and 3 L/min were 104.8 s, 52.4 s, and 34.9 s, respectively.

Surface temperature of helical tube was also measured by an infrared imaging system (Optris, PI200, Germany). Infrared imaging was conducted immediately after each experiment. To do this,

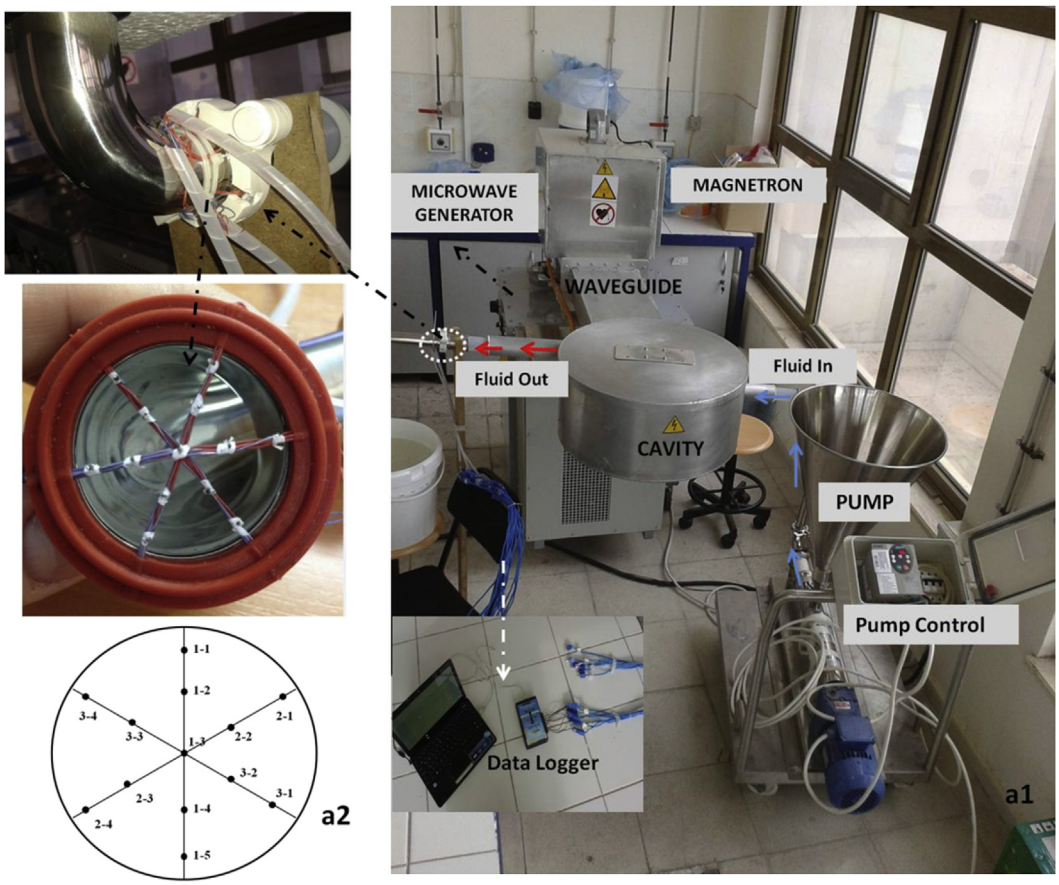

Fig. 1. Continuous flow microwave system (a1) and thermocouple assembly with locations (a2).

cover of the cavity was removed after the run was terminated and IR image of the surface of tube was acquired. An emissivity value of 0.95 was used for the PTFE tube.

Reynolds (Re) and Dean (Dn) numbers for the runs calculated by using Eqs. (4) and (5): were presented in Table 1.

$$Re = \frac{\rho(\overline{u})^{(2-n)}d^n}{8^{n-1}K}\left(\frac{4n}{3n+1}\right) \tag{4}$$

$$Dn = Re\sqrt{d/D} \tag{5}$$

where $\overline{u}$ is average linear velocity of fluid (m/s), n is flow behavior index, K is consistency coefficient (Pa.s^n), ρ is density (kg/m^3), d is inside diameter of tubing (m) and D is helical coil diameter (m). The power absorbed by the fluids was calculated based on inlet and outlet average temperatures and physical properties of the test fluids at room temperature using the calorimetric equation (Eq. (6)). Mass flow rate ($\dot{m}$) was calculated by using volumetric flow rate and density of fluids.

Table 1
Reynolds and Dean numbers of test fluids.

Flow rate	Distilled water		0.5% CMC		1% CMC	
	Re	Dn	Re	Dn	Re	Dn
1 Lpm	556.2	180.8	1.36	0.44	0.14	0.05
2 Lpm	1112.4	361.5	2.39	0.78	0.42	0.14
3 Lpm	1668.6	542.3	3.91	1.27	0.79	0.26

$$q_{abs} = \dot{m}c_p\Delta T \tag{6}$$

2.2.4. Numerical modeling

2.2.4.1. Governing equations. Electromagnetism, heat transfer and fluid flow equations were coupled for numerical modeling of continuous flow microwave heating. Governing equations for these three physics were Maxwell, Fourier and Navier-Stokes, respectively. Maxwell equations were solved to determine electric field distribution in the cavity, waveguide and tubing (Eq. (7)).

$$\nabla \times \left(\frac{1}{\mu'}\nabla \times \vec{E}\right) - \frac{\omega^2}{c}(\varepsilon' - i\varepsilon'')\vec{E} = 0 \tag{7}$$

where μ' is relative permeability of material, $\vec{E}$ is electric field intensity (V/m), ε' is dielectric constant of material, ε'' is relative dielectric loss of material, ω is angular wave frequency (2πf, rad/s). Volumetric heat source was calculated by Eq. (8) using electric field intensity value and dielectric properties.

$$Q = \sigma|\vec{E}|^2 = 2\pi\varepsilon_0\varepsilon''f|\vec{E}|^2 \tag{8}$$

where σ is electrical conductivity of material (S/m), ε_0 is free space permittivity (8.854×10^{-2} F/m) and f is frequency (Hz).

Temperature distribution was calculated using Fourier energy equation (Eq. (9)) including the volumetric heat source term (Q) as energy source.

$$\rho c_p \frac{\partial T}{\partial t} + v\nabla T = \nabla k \nabla T + Q \tag{9}$$

where k is thermal conductivity (W/m.K), ρ is density (kg/m^3), c_p is specific heat (J/kg.K), T is temperature (℃), v is velocity vector (m/s) and Q is electromagnetic heat generation term (W/m^3).

2.2.4.1.1. Continuity, momentum and heat transfer equations in helical tube. Heat transfer equation (Eq. (10)), momentum equations (Eqs. (11)–(13)) and continuity equation (Eq. (14)) for helical coordinate system (Fig. 2) were presented below:

Heat transfer equations,

$$u\frac{\partial T}{\partial r} + \frac{v}{r}\frac{\partial T}{\partial \psi} + \frac{w}{R + r\sin\psi}\frac{\partial T}{\partial \theta} = \frac{\nu}{Pr}\left(\frac{\partial^2 T}{\partial r^2} + \frac{1}{r}\frac{\partial T}{\partial r} + \frac{\sin\psi}{R + r\sin\psi}\frac{\partial T}{\partial r} + \frac{1}{r^2}\frac{\partial^2 T}{\partial \psi^2} + \frac{\cos\psi}{r(R + r\sin\psi)}\frac{\partial T}{\partial \psi} + \frac{1}{(R + r\sin\psi)^2}\frac{\partial^2 T}{\partial \psi^2}\right) + Q \tag{10}$$

Momentum equations,

$$\frac{u}{r}\frac{\partial u}{\partial \psi} + v\frac{\partial u}{\partial r} + \frac{uv}{r} - \varepsilon\omega w\left(w\cos\psi + \lambda\frac{\partial u}{\partial \psi}\right) = -\frac{1}{r}\frac{\partial P}{\partial \psi} + \left[\frac{\partial^2 u}{\partial r^2} + \frac{1}{r}\frac{\partial u}{\partial r} - \frac{u}{r^2} - \frac{1}{r}\frac{\partial^2 v}{\partial r \partial \psi} + \frac{1}{r^2}\frac{\partial v}{\partial \psi}\right] + \varepsilon\omega\left[\eta\sin\psi + \lambda\frac{\partial \alpha}{\partial \psi}\right] \tag{11}$$

$$\frac{u}{r}\frac{\partial v}{\partial \psi} + v\frac{\partial v}{\partial r} + \frac{u^2}{r} - \varepsilon\omega w\left(w\sin\psi + \lambda\frac{\partial v}{\partial \psi}\right) = -\frac{\partial P}{\partial r} + \frac{1}{r^2}\frac{\partial^2 v}{\partial \psi^2} - \frac{1}{r}\frac{\partial^2 u}{\partial r \partial \psi} - \frac{1}{r^2}\frac{\partial u}{\partial \psi} + \varepsilon\omega\left[\eta\cos\psi + \lambda\frac{\partial \gamma}{\partial \psi}\right] \tag{12}$$

$$\frac{u}{r}\frac{\partial w}{\partial \psi} + v\frac{\partial w}{\partial r} + \frac{u^2}{r} + \varepsilon\omega w\left(u\cos\psi + w\sin\psi + \lambda\frac{\partial w}{\partial \psi}\right) = -\omega\frac{\partial P}{\partial s} + \varepsilon\omega\lambda\left(\frac{\partial P}{\partial \psi}\right) + \frac{1}{r^2}\frac{\partial^2 w}{\partial \psi^2} + \frac{1}{r}\frac{\partial w}{\partial r} + \frac{\partial^2 w}{\partial r^2} + \frac{1}{r}\frac{\partial}{\partial \psi}\left[\varepsilon w\omega\cos\psi + \varepsilon\omega\lambda\frac{\partial u}{\partial \psi}\right] + \frac{\partial}{\partial r}\left[\varepsilon w\omega\sin\psi + \varepsilon w\lambda\frac{\partial v}{\partial \psi}\right] + \frac{1}{r}\left[\varepsilon w\omega\sin\psi + \varepsilon\omega\lambda\frac{\partial v}{\partial \psi}\right] \tag{13}$$

Continuity equations,

$$\frac{1}{r}\frac{\partial u}{\partial \psi} + \frac{\partial v}{\partial r} + \frac{v}{r} + \varepsilon\omega\left[u\cos\psi + v\sin\psi - \lambda\frac{\partial w}{\partial \psi}\right] = 0 \tag{14}$$

where α, γ, η, ω unitless values were defined in Eqs. (15)–(18).

$$\alpha = \frac{1}{r}\frac{\partial w}{\partial \psi} + \varepsilon\omega\left(w\cos\psi + \lambda\frac{\partial u}{\partial \psi}\right) \tag{15}$$

$$\gamma = -\frac{\partial w}{\partial \psi} - \varepsilon\omega\left(w\sin\psi + \lambda\frac{\partial v}{\partial \psi}\right) \tag{16}$$

$$\eta = \frac{\partial u}{\partial r} + \frac{u}{r} - \frac{1}{r}\frac{\partial v}{\partial \psi} \tag{17}$$

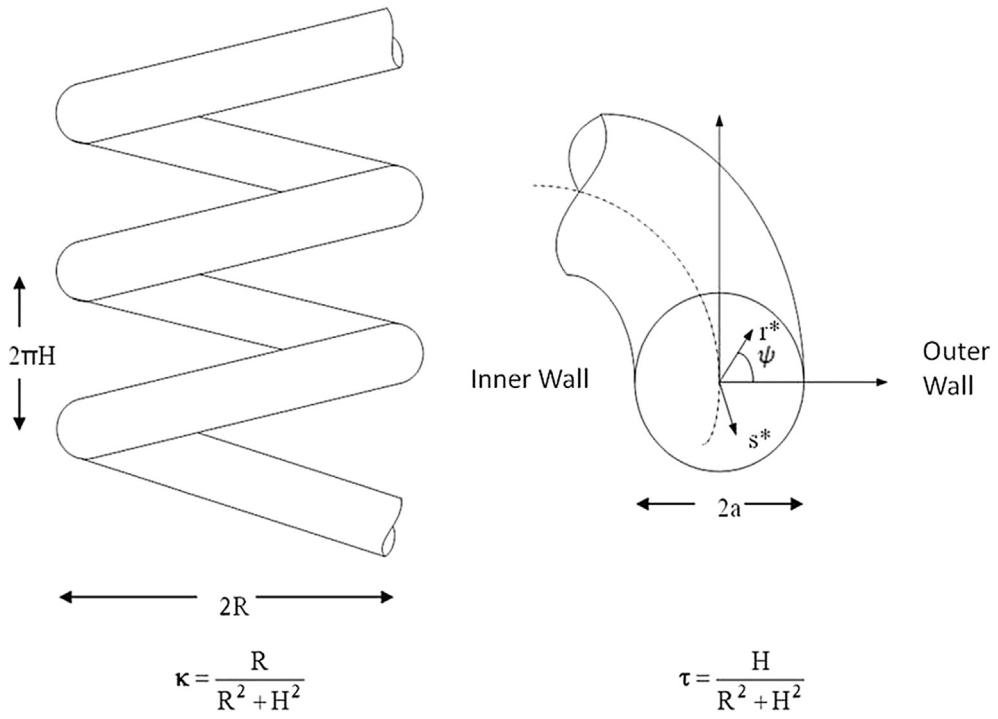

Fig. 2. Helical coordinate system.

$$\omega = \frac{1}{1 + \varepsilon r \sin\psi} \tag{18}$$

u, v, w symbols in momentum equations are dimensionless velocities in *r, ψ, s* directions; P is the dimensionless pressure, and ε and λ are the dimensionless curvature and torsion defined as Eq. (19).

$$r = \frac{r^*}{a}, \quad s = \frac{s^*}{a}, \quad u = \frac{u^*}{\nu/a}, \quad v = \frac{v^*}{\nu/a}, \quad w = \frac{w^*}{\nu/a},$$
$$P = \frac{p^*}{(\rho\nu^2/a^2)}, \quad \varepsilon = \kappa a, \quad \lambda = \frac{\tau}{\kappa} = \frac{H}{R} \tag{19}$$

Assumptions were as follows:

- Fluid was incompressible
- PTFE tubing was assumed completely transparent to microwave
- Minimum reflection was assumed inside the microwave system
- Steady state condition
- Effect of gravity was neglected

2.2.4.2. Development of COMSOL model. COMSOL Multiphysics (V. 4.4, Comsol AB, Stockholm, Sweden) was used for numerical modeling of continuous-flow microwave heating. Radio frequency module was employed for solving Maxwell equations; heat transfer and fluid flow modules were used to solve Fourier and Navier-Stokes equations. These modules were coupled for solving the problem and temperature values were predicted at thirteen locations (the same locations where the thermocouples lie in the assembly). Main steps in model development were geometry building, defining boundary conditions, mesh generation, solving and post processing. Geometry building was performed in 3D as shown Fig. 3.

Temperature dependent thermophysical (thermal conductivity, viscosity, density and specific heat) dielectric (dielectric constant and dielectric loss factor) properties of test fluids were defined inside the tubing, while default thermophysical and dielectric properties of air were used inside the cavity and the waveguide.

Microwave energy source was dominant TE_{10} mode, frequency was 915 MHz and power was 4 kW. This source was supplied at the entry port of the waveguide by assigning port boundary condition. The walls of cavity and waveguide were defined as perfect electric conductors, scattering boundary condition was applied at the inlet and the outlet regions of tubing where fluid enters and exits the cavity.

Heat transfer and momentum balance equations were solved only in the helical tubing domain. Average linear velocities were 0.0147, 0.0294, 0.0441 m/s for the volumetric flow rates of 1, 2, 3 L/min, respectively. No slip boundary condition for fluid flow and convective boundary condition on the wall of helical tubing were defined. A heat transfer coefficient value of 5 W/m^2. K and an ambient temperature of 20 °C were used in the simulations. Atmospheric pressure was set at the outlet of tubing. Temperature of test fluids entering the tubing was 20 °C.

Meshing was performed by using tetrahedral grid in computational domain. Mesh sizes (0.005 m for the tube, 0.03 m for the waveguide and cavity) satisfied the Nyquist criterion (Eq. (20)).

$$S_{max} < \frac{\lambda}{2} = \frac{c}{2f\sqrt{\varepsilon'\mu'}} \tag{20}$$

where λ is the free space wavelength (m), f is the frequency (Hz), c is the speed of light in vacuum (m/s), ε′ is the dielectric constant and μ' is the relative permeability.

Electromagnetic wave equations in Radio Frequency module were solved using frequency domain with GMRES (General Minimum Residual Solver) iterative solver. Stationary solver was used for solving Fourier and Navier-Stokes equations in Heat Transfer and Fluid Flow module using PARDISO (Parallel Direct Linear Solver) direct solver. RF module was coupled with Fluid Flow and Heat Transfer modules in a way that the heat generation terms calculated using RF module were then used to calculate temperature field. Simulations were run on Intel Core i7 2670 QM CPU @ 2.2 GHz (Intel, Santa Clara, CA, USA) processor with 8 GB RAM.

2.2.5. Statistical analysis

Experimental temperature measurements at thirteen points were carried out in duplicate and the average of the two measurements were used to obtain temperature distribution at the exit of cavity. Contour plots for these thirteen temperature readings were produced by linear interpolation using Origin Pro (OriginPro 8.0.0, OriginLab Corporation, Northampton, USA). Predicted temperature values at the same locations were then compared with experimental results and root mean square error (RMSE) values were calculated (Eq. (21)).

$$RMSE = \sqrt{1/N\sum_{i=1}^{N}\left(T_{experimental} - T_{predicted}\right)} \tag{21}$$

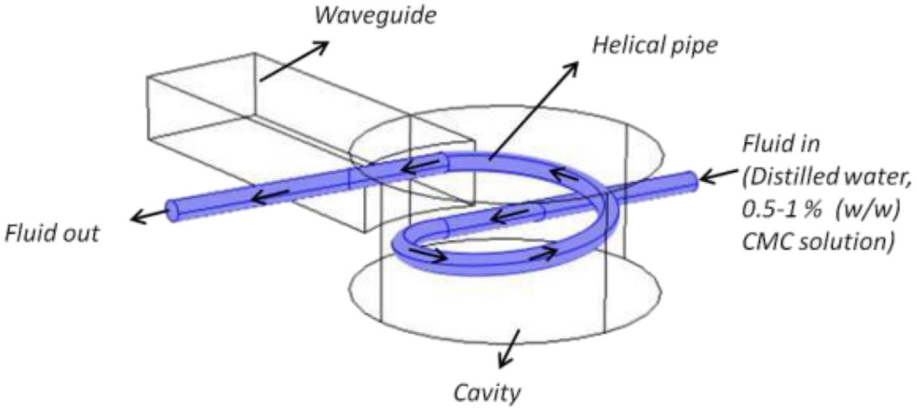

Fig. 3. COMSOL model geometry of continuous flow microwave system in 3D.

3. Results & discussion

3.1. Dielectric, rheological and thermophysical properties of test fluids

Dielectric, rheological and thermophysical properties of test fluids were depicted on Table 2. Dielectric properties describe how materials interact with microwaves, dielectric constant reflects ability to absorb electromagnetic energy, whereas dielectric loss factor is a measure of the ability to convert the absorbed electromagnetic energy into heat. Loss tangent gives information about attenuation of microwave power in foods. Dielectric constant and dielectric loss factor of distilled water both decreased with an increase in temperature. For both CMC solutions, however, dielectric constant decreased while dielectric loss factor increased with increasing temperature. As a result, loss tangent of distilled water almost remain unchanged, while loss tangent of CMC solutions increased with an increase in temperature. This showed that CMC solutions, due to their high loss tangent value, can use microwave energy more effectively in comparison to distilled water and temperature rise would even further enhance this effect. Suitability of tube diameter chosen for heating these test fluids in the current system was evaluated by calculating the penetration depth and it was determined that penetration depth for all test fluids was higher than the tube radius (0.019 m) (Table 2).

Dynamic viscosity of distilled water decreased with an increase in temperature. For CMC solutions, consistency coefficient (K) decreased while flow behavior index (n) increased with trends increasing temperature. Flow behavior index values approaching 1 indicated that CMC solutions behaved more like a Newtonian fluid at higher temperatures. This observation was in agreement with the results of Vais et al. (2001) and Abdelrahim and Ramaswamy (1995).

3.2. Experimental results

Contour plots of cross-sectional temperature distribution at the exit of cavity were shown in Fig. 4. For distilled water; maximum temperature differences were 15.4 °C (62.06–46.65 °C) at 1 L/min, 7.8 °C (41.01–33.21 °C) at 2 L/min, and 6.7 °C (35.27–28.55 °C) at 3 L/min. The highest and lowest temperatures were detected near the tube wall (thermocouple position 1–1 and 1–5, respectively). Maximum cross-sectional temperature differences for 0.5% CMC solution were 28.2 °C (80.12–51.95 °C) at 1 L/min, 10.7 °C (49.35–38.65 °C) at 2 L/min, and 9.4 °C (40.50–31.17 °C) at 3 L/min. The highest temperature was observed at thermocouple position 1–1 while the lowest temperature was at thermocouple location 1–5 for 1 L/min and at thermocouple location 3–2 for 2 and 3 L/min. The maximum temperature differences in the cross section of the tube for 1% CMC solution were 23.3 °C (79.96–56.69 °C) at 1 L/min, 17.7 °C (57.20–39.50 °C) at 2 L/min, and 13.3 °C (43.45–30.17 °C) at 3 L/min. The highest temperature was observed again at thermocouple position 1–1 and the lowest temperature was at thermocouple location 3–1 for 1 L/min and at thermocouple location 3–3 for 2 and 3 L/min. In all cases, it was observed that the temperature was the highest at thermocouple location 1–1 (top of tubing) and milder heating was experienced at the center of tube in comparison to the other thermocouple positions.

Average exit temperatures with standard deviation values for all test fluids at all flow rates were presented in Table 3. Temperature distribution was found to be the most uniform for distilled water at 3 L/min based on the standard deviation values. The uniformity of heating was the lowest for 0.5% CMC solution at 1 L/min. As shown in Table 1, Dean and Reynolds numbers in case of CMC solutions were much lower than those for distilled water at all flow rates. Dean number is an indication of the strength of secondary flow where a high Dean number translates into a greater degree of radial mixing. Austin and Seader (1973) reported that the axial velocity profile across curved tubes was essentially parabolic and unaltered from the fully developed laminar flow profile in straight pipe at low Dean number values (Dn = 1). In fact, a Dean number greater than 10 was necessary in order to create radial mixing. Temperature distribution for distilled water was more uniform than those for 0.5% and 1% CMC solutions owing to the much higher Dean numbers associated with water flow. Parabolic velocity profile essentially did not change when CMC solutions were used (Fig. 9).

Helical tube configuration served another purpose, in addition to creating radial mixing, in the present study. The fluid was

Table 2
Dielectric, thermophysical, rheological properties of test fluids.

Fluid type	T(°C)	ε'^{a}	ε''^{a}	tan δ^{b}	D_p (m)^{c}	k^{d} (W/m °C)	ρ^{e} (kg/m^3)	C_p^{f} (J/kg.K)	μ^{g} (Pa.s)	
Distilled water	20	84.9	4.09	0.048	0.118	0.604	995.7	4178.4	1.005×10^{-3}	
	35	75.8	3.39	0.045	0.134	0.625	992.7	4182.9	0.7228×10^{-3}	
	50	70.0	2.98	0.043	0.147	0.642	987.9	4189.9	0.5494×10^{-3}	
	65	65.7	2.79	0.042	0.152	0.657	981.5	4199.3	0.4355×10^{-3}	
	80	62.3	2.73	0.044	0.151	0.669	973.4	4211.2	0.3565×10^{-3}	
	90	60.4	2.74	0.045	0.148	0.675	967.0	4220.5	0.3165×10^{-3}	
									K (Pa.s^n)	n
0.5% CMC solution	20	77.80	8.91	0.115	0.052	0.602	997.6	4170.3	0.639	0.791
	35	74.14	9.26	0.125	0.049	0.623	994.5	4174.8	0.409	0.844
	50	70.22	10.32	0.147	0.043	0.641	989.8	4181.9	0.246	0.860
	65	66.04	12.11	0.183	0.035	0.656	983.4	4191.4	0.148	0.865
	80	61.60	14.62	0.237	0.028	0.668	975.2	4203.3	0.096	0.906
	90	58.49	16.69	0.285	0.024	0.674	968.9	4212.7	0.062	0.974
									K (Pa.s^n)	n
1% CMC solution	20	77.05	9.07	0.118	0.051	0.601	999.5	4162.1	5.522	0.449
	35	73.52	9.23	0.126	0.049	0.622	996.4	4166.8	2.722	0.652
	50	69.73	10.11	0.145	0.043	0.640	991.7	4173.9	1.621	0.753
	65	65.67	11.70	0.178	0.036	0.655	985.2	4183.4	0.953	0.781
	80	61.36	14.02	0.228	0.029	0.667	977.1	4195.4	0.453	0.785
	90	58.33	15.97	0.274	0.025	0.673	970.8	4204.8	0.285	0.885

[a]Komarov&Tang (2004) for distilled water, Coronel et al. (2008) for CMC solutions,[b] Eq. (1), [c] Eq. (2), [d,e,f] Choi&Okos equations (Toledo, 1994), [g]Geankoplis (1993) and K, n values were determined experimentally for CMC solutions.

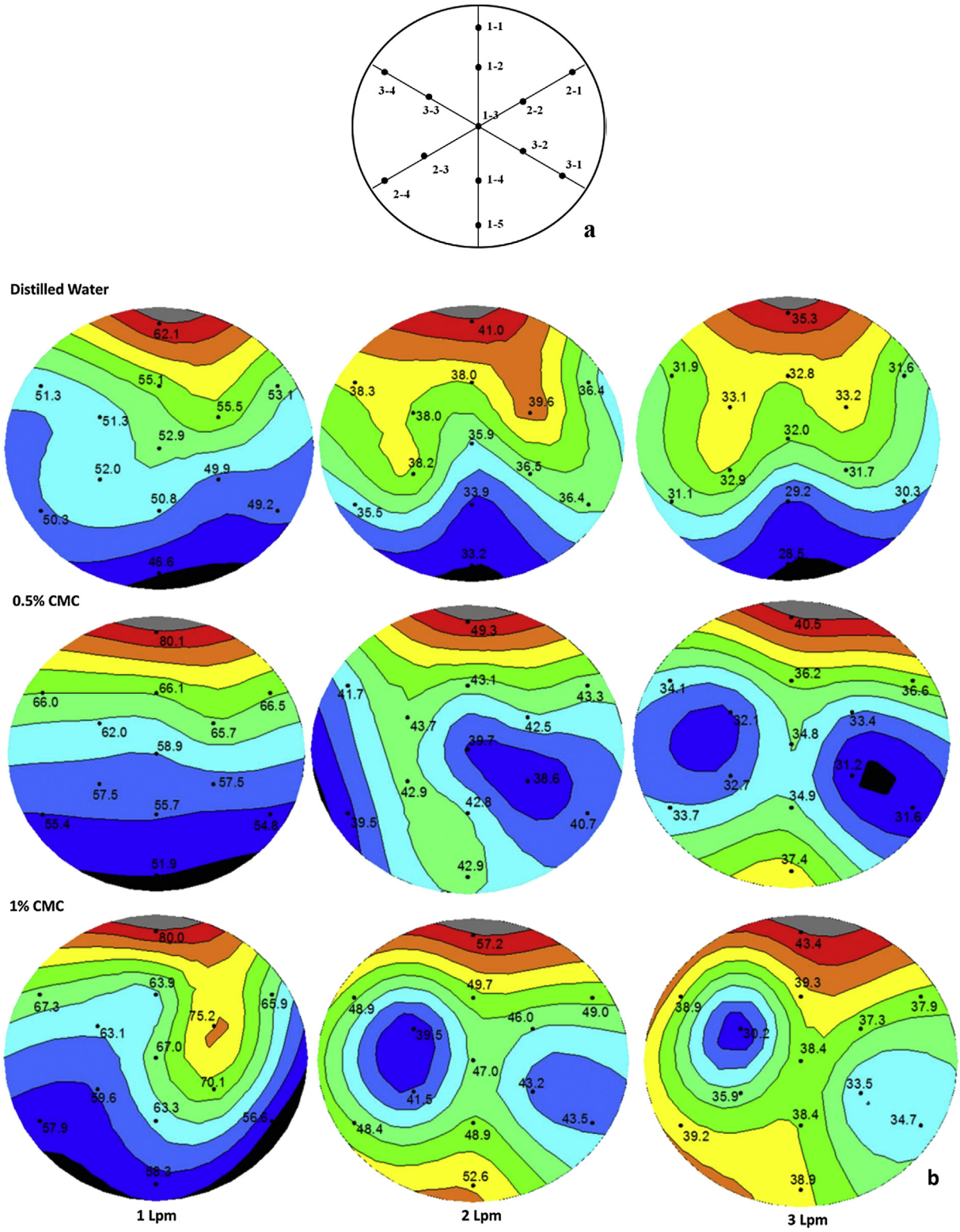

Fig. 4. Position of thirteen thermocouples (a), Experimental contour plots of cross-sectional temperature distribution at the exit of tube at different flow rates (b).

exposed to varying electric field strengths as it moved along thanks to the curving path of the helical tube. Since secondary flow effect was absent during the flow of CMC solutions, it was this effect (turntable effect) which improved the uniformity of heating. However, both effects played a role in improving heating uniformity in case of distilled water.

Distilled water experienced a lower temperature increase when compared to the CMC solutions for all flow rates (Table 3) due to the lower loss tangent of distilled water. This also resulted in inefficient use of available microwave energy by distilled water. Penetration

Table 3
Experimental and simulated average exit temperature and absorbed microwave energy values.

Fluid type	Flow rate (L/min)	Temperature				Absorbed microwave energy		
		RMSE (°C)[a]	$T_{avg,exp}$ (°C)[b]	$T_{avg,sim}$ (°C)	% Error [c]	$q_{abs,exp}$ (W)	$q_{abs,sim}$ (W)	% Error[c]
Distilled water	1	9.1	52.3 ± 3.8	44.0	15.9	2230.7	1657.5	25.7
	2	3.9	37.0 ± 2.2	33.8	8.7	2355.2	1911.9	18.8
	3	2.7	31.8 ± 1.8	29.9	1.1	2450.0	2060.0	16.1
0.5% CMC solution	1	13.7	61.4 ± 7.5	72.2	−17.6	2859.1	3605.0	−26.1
	2	3.2	42.4 ± 2.7	43.3	−2.1	3103.2	3227.9	−4.0
	3	2.2	34.6 ± 2.6	35.3	−2.0	3037.0	3182.6	−4.8
1% CMC solution	1	12.5	65.3 ± 6.9	75.0	−14.9	3128.2	3798.1	−21.4
	2	3.5	47.3 ± 4.7	45.7	3.4	3781.8	3560.2	5.9
	3	3.5	37.4 ± 3.2	35.1	6.1	3619.2	3140.8	13.3

[a] Calculated using Eq. (21) using the predicted and experimentally measured temperatures at thirteen locations.
[b] Average and standard deviation of experimentally measured temperatures at thirteen locations.
[c] % Error = 100*(experimental value − simulated value)/experimental value.

depth is also an indicator for efficiency of heating by electromagnetic energy. A penetration depth larger than the diameter of tube for example indicates poor absorption of microwave energy by the material (significant part of electromagnetic energy cannot be used by the material) (Buffler, 1993; Muley and Boldor, 2012). As shown in Table 2, penetration depth for distilled water was much larger than the tube diameter when compared to CMC solutions which indicates poor absorption of energy by distilled water. Absorbed microwave energy values for the test fluids presented in Table 3 also shows that the microwave energy was used more efficiently by the CMC solutions.

Thermal images of the helical tube surface captured by the infrared camera were shown in Fig. 5 (maximum temperature values along the surface of pipe were shown at the upper right corner of the images, and dashed lines show the borderline of the helical tube). Temperatures at seven locations measured along the tube surface were depicted on Fig. 6a. According to the thermal images, temperature on the tube surface was the highest just before the tube exited the cavity as expected. This region on the helical tube was closest to the thermocouple location 1–1 where the highest temperature was measured experimentally for all test fluids at all flow rates. In spite of the fact that infrared camera measured the tube surface temperature while the thermocouples measured temperature of the fluid, a close agreement between these two measurements was observed (Figs. 4 and 6a). A much greater temperature increase was experienced between points 6 and 7 in comparison to those observed between other points especially at 1 L/min (the lowest flow rate used in the study). This was presumably due to the exposure of the fluid to an electromagnetic energy that was more concentrated in this region due to the addition of the energy reflected from the top cover of the cavity. This was because the distance between the tube and the top cover became smaller toward the exit. Since the residence time of the fluid in the intense-energy region increased with decreasing flow rate, temperature increase observed at 1 L/min was larger than those occurred for higher flow rates.

Results of the present study and those of previous studies which employed different microwave and radio frequency systems were compared in terms of heating uniformity. Temperature distribution achieved in the present study was more uniform than that observed by Zhong et al. (2003) who studied heating of 1% CMC solution at different flow rates (7.56 L/min, 15.12 L/min, 22.68 L/min) in a continuous-flow radio frequency system (frequency 40.68 MHz, power 30 kW). In that study temperature differences between center and wall of pipe were 20 °C, 14 °C and 10 °C at 7.56 L/min, 15.12 L/min, 22.68 L/min flow rates and those were 12.9 °C, 10.2 °C, 5.0 °C at 1 L/min, 2 L/min and 3 L/min flow rates in current design. A lower temperature differences were observed in the present study although lower flow rates compared to that of Zhong et al. (2003). Continuous-flow heating of 0.5% CMC solution was studied by Salvi et al. (2009) at different flow rates and at a power of 4 kW in a microwave system (915 MHz, max power 5 kW) designed to focus electromagnetic energy to the center of the straight tube running through the center of the system's elliptical cavity. The maximum cross-sectional temperature difference reported at 1 L/min in their study (60 °C) was much higher that was observed in the present study under the same conditions (~28 °C). A greater average temperature increase was also achieved in the present study (41.4 °C) when compared to that of Salvi et al. (2009) (35 °C). Temperature increase and distribution in case of water however were found comparable in both studies. These explanations are important in terms of showing the advantage of the current design over the other designs studied previously by other researchers.

3.3. Numerical simulation results

3.3.1. Electric field distribution

Surface plots of the electric field distribution within the system were shown for all test fluids in Fig. 7. Predicted electric field strength values were found to vary in the range of 7.0-46,900 V/m for distilled water; 5.9-37,629 V/m for 0.5% CMC solution; 7.9-36,523 V/m for 1% CMC solution. Electric field strength along the helical tube surface was in the range of 783.3-37,333 V/m for distilled water; 666.5-28,967 V/m for 0.5% CMC solution; 523.9-28,186 V/m for 1% CMC solution (left bottom sides of Fig. 7-a,b,c). Volumetric heat generation along the tube (right bottom sides of Fig. 7-a,b,c) was computed to be in the range of 1.62×10^{3}-2.13×10^{6}; 3.68×10^{4}-3.34×10^{6}; 2.38×10^{4}-3.67×10^{6} W/m^3 for distilled water, 0.5% CMC and 1% CMC solution, respectively. Effect of flow rate on temperature change related with volumetric heat generation inside helical tube. Minimum and maximum heat generation at 1, 2, 3 L/min were respectively 7.5×10^{3}-6.2×10^{6} W/m^3, 8.2×10^{3}-6.6×10^{6} W/m^3, 8.6×10^{3}-6.7×10^{6} W/m^3 for distilled water; 3.9×10^{4}-10.9×10^{6} W/m^3, 3.8×10^{4}-10.1×10^{6} W/m^3, 3.7×10^{4}-9.9×10^{6} W/m^3 for 0.5% CMC solution; 2.7×10^{4}-10.9×10^{6} W/m^3, 2.6×10^{4}-10.1×10^{6} W/m^3, 2.5×10^{4}-9.9×10^{6} W/m^3 for 1% CMC solution.

Maximum electric field strength values in the microwave system and along the helical tube were similar for 0.5% and 1% CMC solution were lower than those for distilled water. This difference between distilled water and CMC solutions may be attributed to the tangent loss factor which was directly proportional to the absorbed microwave energy as stated by Zhu et al. (2007a). For the same dielectric constant, larger power absorption results from a larger

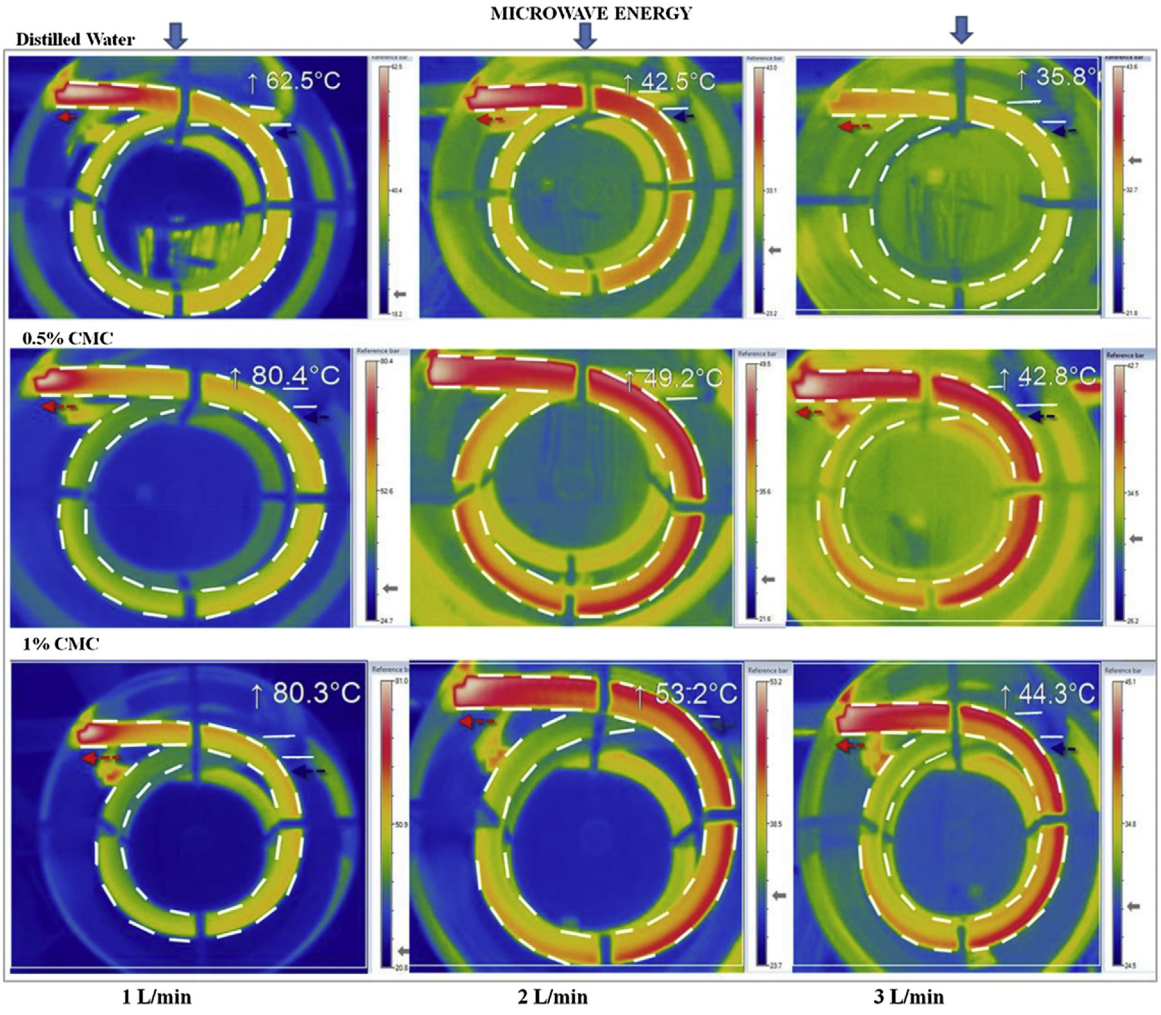

Fig. 5. Thermal images of test fluids at different flow rates.

tangent loss factor and a smaller reflection coefficient (Zhu et al., 2007b). In the present study, larger power absorption during heating of CMC solutions can be explained by the smaller reflection coefficient. Closer values of penetration depth and pipe diameter may have caused better power absorption by CMC solutions. Experimentally calculated absorbed microwave power values (Table 3) showed microwave power absorption of CMC solutions was higher than distilled water as expected with predicted electric field results.

3.3.2. Temperature distribution and total absorbed power

Experimental and simulated temperature, microwave energy absorption values for all test fluids and RMSE values were shown in Table 3. Simulated average exit temperature and absorbed microwave power values for distilled water were lower than those experimentally observed at all flow rates. Estimation of average exit temperature and microwave absorption values for 0.5% and 1% CMC solutions were lower than experimental results at 1 L/min, but higher than observed values at 2 L/min and 3 L/min flow rates. The RMSE values at 1 L/min flow rate were higher than 2 L/min and 3 L/min for all test fluids showing that simulated results better agreed the experimental ones at the higher flow rates. Cuccurollo et al. (2014) also reported that at higher flow rates increased reliability of the computational model developed by COMSOL Multiphysics improved. The time needed to reach the steady state condition at 1 L/min (about 10 min) was longer than that needed at 2 L/min and 3 L/min (about 5 min) for all test fluids. Long come-up time to reach steady state condition resulted in warming up of the cooling water at low flow rates during experiments that may have caused insufficient cooling of the magnetron. Meredith and Metaxas (1993) reported that change in temperature around magnetron may change frequency and hence temperature distribution within material. In light of this discussion, it is possible to say that frequency fluctuations may have been responsible for higher discrepancies between simulated and experimental results at 1 L/min.

Numerical cross-sectional temperature distribution at the exit of tube was shown in Fig. 8. Cross-sectional maximum temperature differences at the outlet of the helical tube for distilled water were 1.6 °C (44.7–43.1 °C) at 1 L/min, 0.9 °C (34.3–33.4 °C) at 2 L/min, and 0.8 °C (30.4–29.6 °C) at 3 L/min. The highest and the lowest predicted temperatures in distilled water for 1 L/min were detected at thermocouple position 1–5 and 2–4; for 2 L/min, 3 L/min at thermocouple positions of 3–1 and 2–4, respectively. Cross-sectional maximum temperature differences at the exit of the helical tube for 0.5% CMC solution were 17.8 °C (82.3–64.5 °C) at 1 L/min, 9.7 °C (48.8–39.1 °C) at 2 L/min, and 7.2 °C (39.4–32.2 °C) at 3 L/min. The temperature differences in the cross section of the tube for %1 CMC solution were 17.2 °C (84.3–67.1 °C) at 1 L/min,

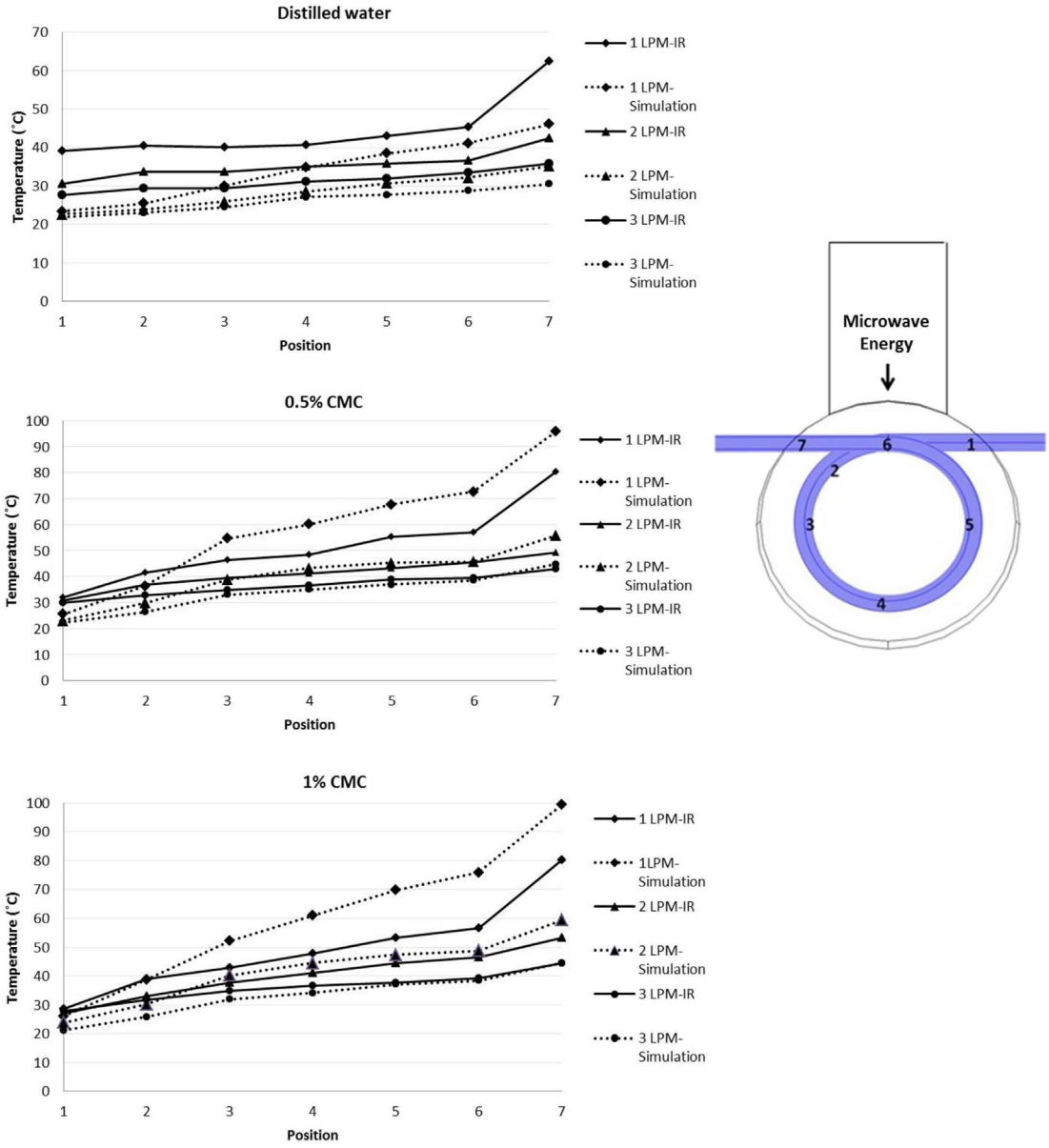

Fig. 6. Temperature values at seven points along the helical tube surface, obtained from thermal (IR) images and simulation results.

9.9 °C (51.3–41.4 °C) at 2 L/min, and 7.1 °C (39.0–31.9 °C) at 3 L/min. The highest and the lowest predicted temperature values in 0.5% and 1% CMC solutions at all flow rates were observed at thermocouple positions 1–5 and 3–3, respectively. Although the highest temperature values were predicted at thermocouple position 1–5 for both CMC solutions (which was 1–1 experimentally), temperature values at 1–1 (top of tube) and 1–5 (bottom of tube) points were very close to each other. At all thermocouple positions, predicted temperature values were lower than the experimental ones for distilled water and maximum temperature differences were less than the observed results at all flow rates.

However, low RMSE values (especially at higher flow rates) were found for test fluids, hot and cold points differed from the experimental results. Constant magnetron frequency was used in the simulations although frequency may have fluctuated during the experiments. Soltysiak et al. (2010) reported that using constant magnetron frequency may not reflect real microwave heating situation which may have been the case in the present study. Variation in magnetron frequency may have changed electric field distribution inside the cavity with a possible change in temperature field in fluid. Since magnetron frequency typically deviates by 50 MHz, applying constant magnetron frequency in the model may result in discrepancies between experimental and simulated temperatures (Soltysiak et al., 2010; Santos et al., 2010; Pitchai et al., 2012; Resurrecion et al., 2015).

Predicted temperature values at seven points along the helical tube surface were depicted on Fig. 6b. These values showed that predicted temperature rise was similar with experimental results as seen in Fig. 6-a,b however the same temperature increase was observed at the bottom of tube in predicted results (which was 1–5 point in Fig. 1-a2). Dotted lines on Fig. 7-a,b showed that sudden increase in volumetric heat generation value occurred at the exit of tube and this effect on temperature was also seen for CMC solutions.

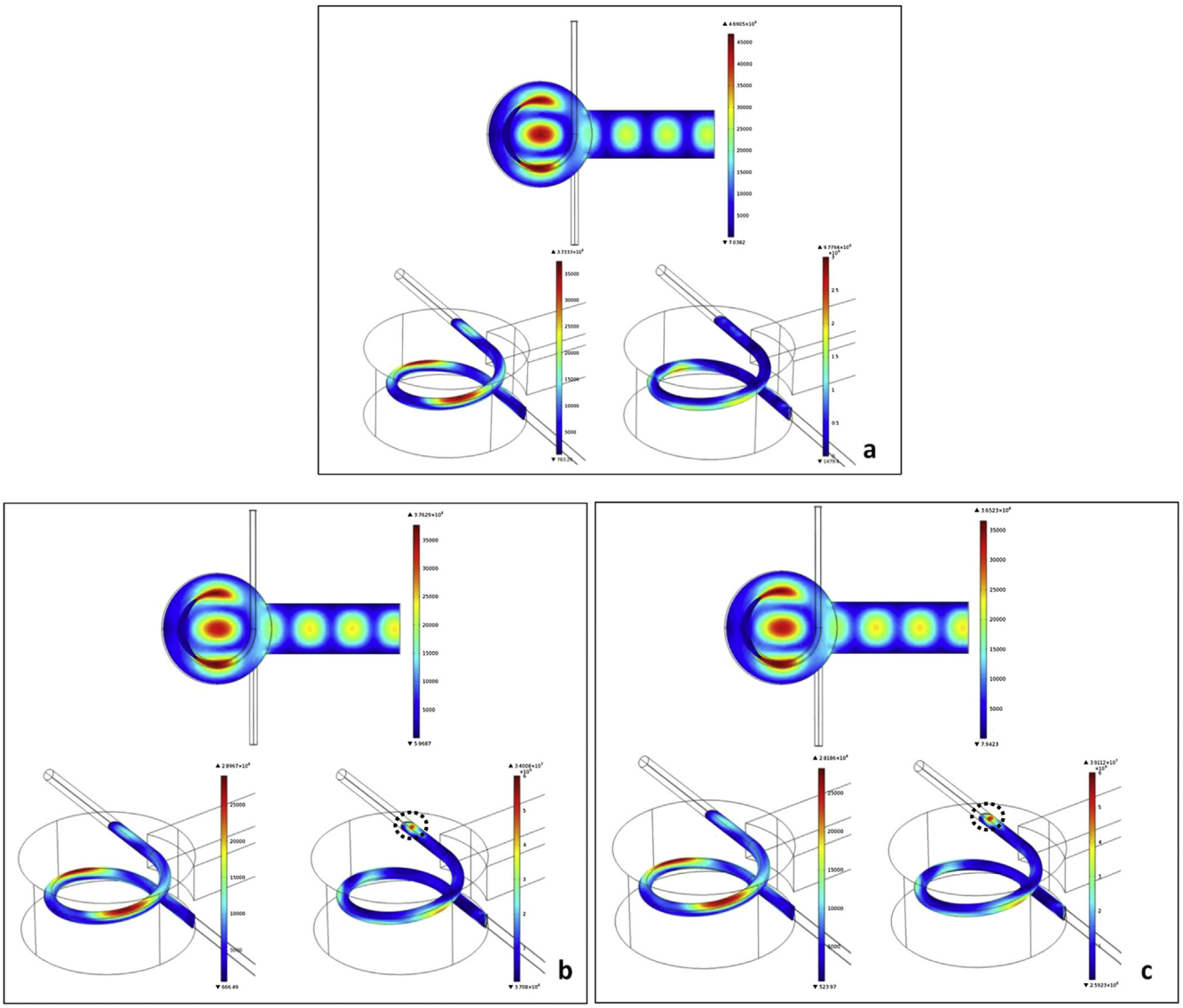

Fig. 7. Electric field distribution in microwave system (top), electric field distribution (bottom left) and heat generation (bottom right) along the helical tube, a) Distilled water b) 0.5% CMC solution c) 1% CMC solution.

3.3.3. *Velocity profiles*

Velocity profiles of the test fluids at 2 L/min were shown in Fig. 9 (similar profiles were observed for other flow rates). It can be seen from the figure that maximum velocity region was thrown outward in case of distilled water, whereas it did not shift in case of CMC solutions. In experimental results, lower standard deviation values for distilled water were attributed to high Dean numbers and the development of secondary flow. Bean-shaped flow profile predicted numerically shows that appreciable secondary flow developed in distilled water, which was in agreement with the experimental observations. No change in axial velocity profile during flow of CMC solutions showed that no mixing effect was achieved. This was expected due to low Dean number values (Dn < 1.3) associated with the flow of these viscous solutions.

4. Conclusion

In this study, a continuous-flow microwave system designed for uniform heating of high-viscosity fluid food products was numerically modeled and the model was experimentally validated. A larger temperature increase, but a lower temperature uniformity was achieved for CMC solutions than for distilled water. Enhanced secondary flow and the resultant radial mixing was responsible for more uniform heating of distilled water. Despite the lack of mixing effect in case of CMC solutions, more uniform temperature distribution was observed in the current design due to the turntable effect when compared to the other existing systems reported in the literature. Uniformity of heating for CMC solutions can be further enhanced by increasing the curvature ratio of helical tube which will in turn enhance the secondary flow effect. Increasing the tube length will also result in better utilization of microwave energy and hence a greater temperature increase. Further studies on the effect of different dielectric and rheological properties are planned with real fluid foods.

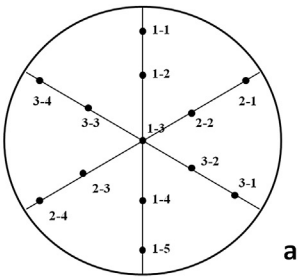

a

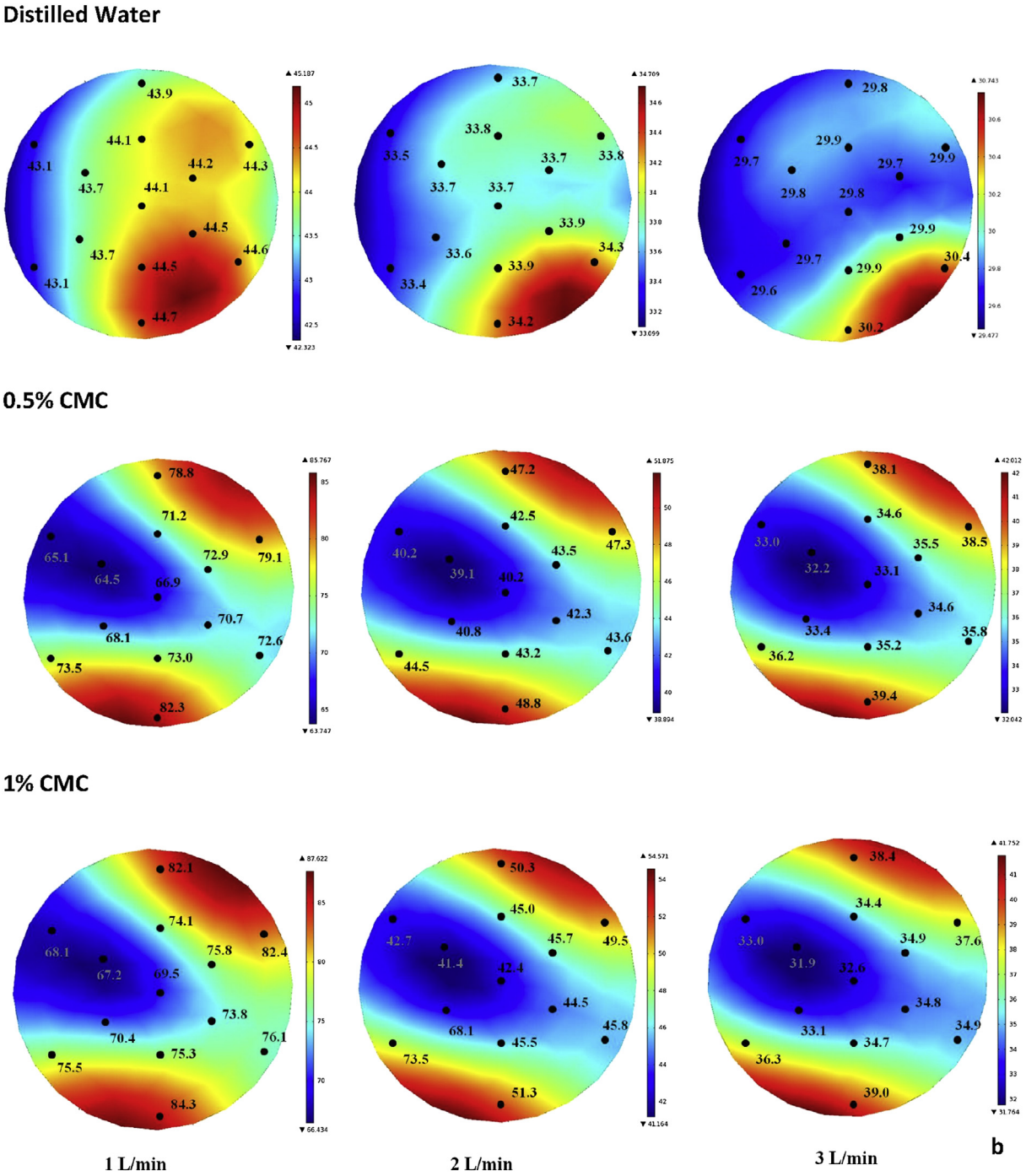

Fig. 8. a) Position of thirteen thermocouples b) Simulated contour plots of cross-sectional temperature distribution at the exit of tube at different flow rates.

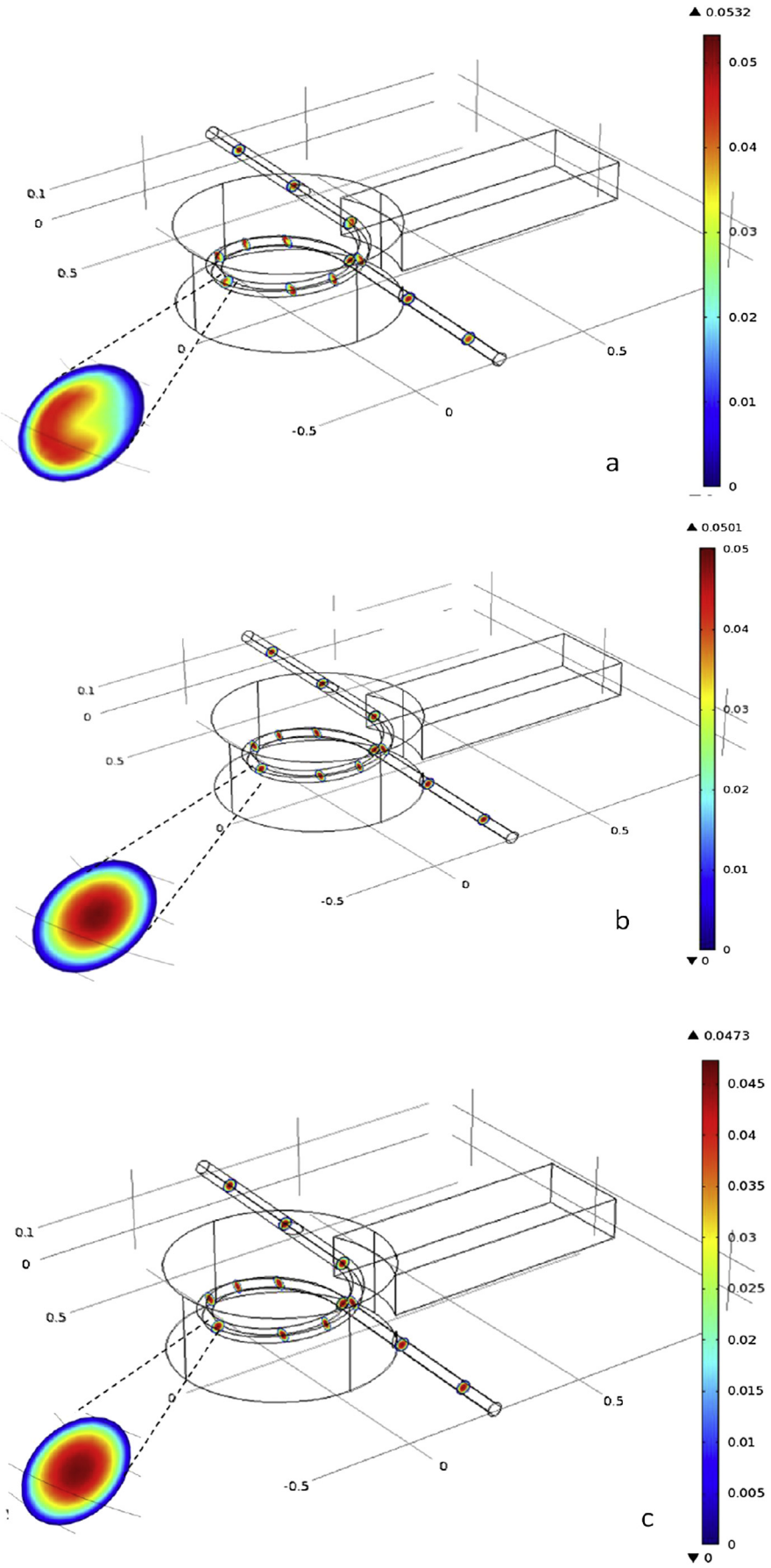

Fig. 9. Velocity profiles of distilled water (a) 0.5% CMC solution (b) 1% CMC solution (c) at 2 L/min flow rate.

Acknowledgements

This research was supported by Mersin University (Project no. BAP-FBE GMB (ST) 2012-2 DR).

References

Abdelrahim, K.A., Ramaswamy, H.S., 1995. High temperature/pressure rheology of carboxymethyl cellulose (CMC). Food Res. Int. 28 (3), 285–290.
Austin, L.R., Seader, J.D., 1973. Fully developed viscous flow in coiled circular pipes. AIChE J. 19 (1), 85–94.
Buffler, C.R., 1993. Microwave Cooking and Processing, pp. 56–77. New York.
Castelain, C., Legentilhomme, P., 2006. Residence time distribution of a purely viscous non-Newtonian fluid in helically coiled or spatially chaotic flows. Chem. Eng. J. 120, 181–219.
Coronel, P., Simunovic, J., Sandeep, K.P., 2003. Temperature profiles within milk after heating in a continuous-flow tubular microwave system operating at 915 MHz. J. Food Sci. 68 (6), 1976–1981.
Coronel, P., Truong, V., Simunovic, J., Sandeep, K.P., Cartwright, G.D., 2005. Aseptic processing of sweetpotato purees using a continuous flow microwave system. J. Food Sci. 70 (9), 531–536.
Coronel, P., Simunovic, J., Sandeep, K.P., Cartwright, G.D., Kumar, P., 2008. Sterilization solutions for aseptic processing using a continuous flow microwave system. J. Food Eng. 85, 528–536.
Cuccurollo, G., Giordano, L., Viccione, G., 2014. A fast and accurate hybrid model for simulating continuous pipe flow microwave heating of liquids. Int. J. Mech. 8, 45–52.
Eesa, M., 2009. CFD Studies of Complex Fluid Flows in Pipes. The University of Birmingham. Phd thesis.
Geankoplis, C.J., 1993. Transport Processes and Unit Operations, third ed. USA.
Gentry, T.S., Roberts, J.S., 2005. Design and evaluation of a continuous flow microwave pasteurization system for apple cider. Lwt Food Sci. Technol. 38 (3), 227–238.
Komarov, V.V., Tang, J., 2004. Dielectric permittivity and loss factor of tap water at 915 MHz. Microw. Opt. Technol. Lett. 42 (5), 419–420.
Koutsky, J.A., Adler, R.J., 1964. Minimization of axial dispersion by use of secondary flow in helical tubes. Can. J. Chem. Eng. 239–246.
Kumar, V., Saini, S., Sharma, M., Nigam, K.D.P., 2006. Pressure drop and heat transfer study in tube-in-tube helical heat exchanger. Chem. Eng. Sci. 61, 4403–4416.
Kumar, P., Coronel, P., Truong, V.D., Simunovic, J., Swartzel, K.R., Sandeep, K.P., Cartwright, G., 2008. Overcoming issues associated with the scale-up of a continuous flow microwave system for aseptic processing of vegetable purees. Food Res. Int. 41, 454–461.
Meredith, A.C., Metaxas, R.J., 1993. Industrial Microwave Heating. London, UK.
Muley, P.D., Boldor, D., 2012. Multiphysics numerical modeling of the continuous flow microwave-assisted transesterification process. J. Microw. Power Electromagn. Energy 46 (3), 139–162.
Nikdel, S., MacKellar, D.G., 1992. A microwave system for continuous pasteurization of orange juice. Proc. Fla. State Hort. Soc. 105, 108–110.
Nikdel, S., Chen, C.S., Parish, M.E., Mackellar, D.G., Friedrich, L.M., 1993. Pasteurization of citrus juice with microwave-energy in a continuous-flow unit. J. Agric. Food Chem. 41 (11), 2116–2119.
Palazoğlu, T.K., Sandeep, K.P., 2004. Effect of tube curvature ratio on the residence time distribution of multiple particles in helical tubes. Lebensm.-Wiss. Technol. 37, 387–439.
Pitchai, K., Birla, S.L., Subbiah, J., Jones, D., Thippareddi, H., 2012. Coupled electromagnetic and heat transfer model for microwave heating in domestic ovens. J. Food Eng. 112, 100–111.
Resurrecion Jr., F.P., Luan, D., Tang, J., Liu, F., Tang, Z., Pedrow, P.D., Cavalieri, R., 2015. Effect of changes in microwave frequency on heating patterns of foods in a microwave assisted thermal sterilization system. J. Food Eng. 150, 99–105.
Romano, V., Apicella, R., 2015. Microwave heating of liquid foods. Engineering 7, 297–306.
Salvi, D., Ortego, J., Arauz, C., Sabliov, C.M., Boldor, D., 2009. Experimental study of the effect of dielectric and physical properties on temperature distribution in fluids during continuous flow microwave heating. J. Food Eng. 93 (2), 149–157.
Santos, T., Costa, L.C., Valente, M., Monteiro, J., Sousa, J., 2010. 3D electromagnetic field simulation in microwave ovens: a tool to control thermal runaway. In: COMSOL Conference, Paris.
Sierra, I., Vidal-Valverde, C., Olano, A., 1999. The effects of continuous flow microwave treatment and conventional heating on the nutritional value of milk as shown by influence on vitamin B1 retention. Eur. Food Res. Technol. 209, 352–354.
Soltysiak, M., Erle, U., Celuch, M., 2010. Influence of the magnetron operating frequency on the results of microwave heating. In: Microwave Symposium Digest, Anaheim.
Steed, L.E., Truong, V.D., Simunovic, J., Sandeep, K.P., Kumar, P., Cartwright, G.D., Swartzel, K.R., 2008. Continuous flow microwave-assisted processing and aseptic packaging of purple-fleshed sweetpotato purees. J. Food Sci. 73 (9), 455–462.
Tajchakavit, S., Ramaswamy, H.S., 1995. Continuous-flow microwave-heating of orange juice – evidence of nonthermal effects. J. Microw. Power Electromagn. Energy 30 (3), 141–148.
Tajchakavit, S., Ramaswamy, H.S., Fustier, P., 1998. Enhanced destruction of spoilage microorganisms in apple juice during continuous flow microwave heating. Food Res. Int. 31 (10), 713–722.
Thostenson, E.T., Chou, T.W., 1999. Microwave processing: fundamentals and applications. Compos. Part A Appl. Sci. Manuf. 30 (9), 1055–1071.
Toledo, R.T., 1994. Fundamentals of Food Process Engineering, second ed., pp. 233–235 New York, USA.
Vais, A.E., Palazoglu, T.K., Sandeep, K.P., Daubert, C.R., 2001. Rheological characterization of carboxymethylcellulose solution under aseptic processing conditions. J. Food Process Eng. 25, 41–61.
Valero, E., Villamiel, M., Sanz, J., Martinez-Castro, I., 2000. Chemical and sensorial changes in milk pasteurised by microwave and conventional systems during cold storage. Food Chem. 70, 77–81.
Villamiel, M., Lopez Fandiño, R., Corzo, N., Martinez-Castro, I., Olano, A., 1996. Effects of continuous flow microwave treatment on chemical and microbiological characteristics of milk. Lebensm. Unters. Forsch. 202, 15–18.
Zhong, Q., Sandeep, K.P., Swartzel, K.R., 2003. Continuous flow radio frequency heating of water and carboxymethylcellulose solutions. J. Food Sci. 68 (1), 217–223.
Zhu, J., Kuznetsov, A.V., Sandeep, K.P., 2007a. Numerical simulation of forced convection in a duct subjected to microwave heating. Heat Mass Transf. 43, 255–264.
Zhu, J., Kuznetsov, A.V., Sandeep, K.P., 2007b. Mathematical modeling of continuous flow microwave heating of liquids (effects of dielectric properties and design parameters). Int. J. Therm. Sci. 46, 328–341.